Science Bulletin 64 (2019) 469–477

Contents lists available at ScienceDirect

Science Bulletin

journal homepage: www.elsevier.com/locate/scib

Article

Operation of silicon-germanium heterojunction bipolar transistors with different structures at deep cryogenic temperature

Guofang Yu [a,b], Renrong Liang [a,b,*], Xiawa Wang [a,b], Jun Xu [a,b], Tian-Ling Ren [a,b]

[a] Institute of Microelectronics, Tsinghua University, Beijing 100084, China
[b] Beijing National Research Center for Information Science and Technology (BNRist), Tsinghua University, Beijing 100084, China

ARTICLE INFO

Article history:
Received 9 January 2019
Received in revised form 18 February 2019
Accepted 25 February 2019
Available online 7 March 2019

Keywords:
SiGe HBTs
Quantum computing
Cryogenic temperature
Analytical model

ABSTRACT

In this work, the device performances of discrete and integrated SiGe heterojunction bipolar transistors (HBTs) with different device structures from 300 to 4.8 K were investigated. The turn-on voltages of base-emitter and base-collector junctions increased non-linearly with temperature cooled to 4.8 K. Energy bandgap engineering was taken into account for the analytical model of the turn-on voltage versus temperature. Incomplete ionization occurred in the base-collector junction because of the low doping concentration. The trap-assisted tunneling current in the forward base current was clearly observed below 20 K. The ideality factor and saturation current were shown to be temperature dependence. The ideality factor was much larger than 2 below 40 K, indicating that the current is not only contributed by drift, diffusion and recombination, but also by tunneling. The peak current gain of the discrete SiGe HBTs achieved the maximum value of 3,388 at 80 K, while that of the integrated was 546 at 140 K. The transconductance in logarithm was linearly dependent on reciprocal temperature above 50 K, but flattened below 50 K. Early effect was evidently observed below 77 K in the fixed base current output characteristics of the discrete SiGe HBTs, and it was not obvious for the integrated SiGe HBTs.

1. Introduction

Silicon-germanium heterojunction bipolar transistor (SiGe HBT) technology is a promising solution for cryogenic temperature applications [1–6] due to the excellent current gain, radio frequency (RF) response and noise performance over an extremely wide range of temperature [7]. It is well known that silicon bipolar transistors are not suitable for cryogenic applications because of the heavy doping effects and carrier freeze-out at cryogenic temperature [8]. SiGe HBTs, in contrast, exhibit enhanced performance at low temperature because of bandgap engineering [9].

Previously, III-V high electron mobility transistors (HEMTs) have been successfully demonstrated for cryogenic circuit applications [10–19], which exhibit excellent transistor-like behavior at cryogenic temperature. Unfortunately, the III-V semiconductor technology is incompatible with Si complementary metal-oxide-semiconductor (CMOS) technology and cannot be integrated [20]. Therefore, the seamless compatibility of SiGe HBT technology with the conventional Si CMOS technology is the most important advantage over the III-V technology [20–23]. Recently, Sander and co-workers [24–28] have developed plentiful researches about cryogenic SiGe low-noise amplifiers (LNAs). Curry et al. [29] examined a discrete, commercial SiGe HBT for cryogenic preamplification of a single electronic transistor.

Moreover, Cressler and co-workers [8,21–23,30,31] presented the direct current (DC) measurements of the IBM 1st to 4th generation SiGe HBTs operating in cryogenic temperature regime. Especially, a highly scaled 90 nm SiGe HBT operating at temperature as low as 70 mK has been demonstrated [23]. These results show that SiGe HBT has overwhelming advantages over Si bipolar junction transistor (BJT) at extremely low temperature regime. However, the discrepancy of DC characteristics (such as the current gain and transconductance) at wide temperature range between different configurations had seldom been discussed in the previous works. Therefore, it is urgent to study the impact of different device structures on device performances at cryogenic temperature.

In this work, we investigated the performances of a discrete SiGe HBT and an integrated SiGe HBT with different structures operating from 300 to 4.8 K. In Section 2, the device fabrication and structure characterization are presented. In Section 3, an analytical model of the turn-on voltage for base-emitter (BE) and base-collector (BC) junctions is developed and validated. In addition, we

* Corresponding author.
E-mail address: liangrr@mail.tsinghua.edu.cn (R. Liang).

https://doi.org/10.1016/j.scib.2019.03.005
2095-9273/

examined the incomplete ionization effect. The detailed comparisons of device performance are given in Section 4. In Section 5, we discuss the analytical model limitations and draw the conclusions.

2. Device fabrication and structure characterization

Two distinct types of SiGe HBTs have been designed and fabricated, i.e., discrete and integrated structures, which are named as Sample 1 and Sample 2, respectively. As shown in Fig. 1, both types of the HBTs have the typical layout configuration with one emitter and two base regions. The device had a heavily doped poly-Si emitter, an ultra-thin SiGe base layer with heavy boron doping, a lightly doped n-type collector, and a heavily boron doped extrinsic base. The SiGe alloys have grown by reduced pressure chemical vapor deposition (Applied Materials Centura-Epi 200). Pure germane (GeH_4) diluted at 15% in H_2 was used as the source of Ge and dichlorosilane (SiH_2Cl_2) was used as the source of Si. During the epitaxial process, the growth rate and temperature were optimized to decrease the surface roughness and minimize the threading dislocations and point defects.

The schematic cross section of Sample 1 is shown in Fig. 1a. The collector is on the backside of the Si wafer. The total emitter area A_E was designed to be 216 μm^2 with a single emitter area of 0.85 μm × 16 μm. For the SiGe alloy base region, the thickness was about 55 nm, the boron doping concentration was around 4.5×10^{19} cm^{-3}, and the Ge composition was about 0.17. Sample 2 was designed as the integrated device, in which the collector was at the front side of the Si wafer, as show in Fig. 1b. The transistor had an emitter geometry of 0.25 μm × 1.1 μm. The Ge composition and thickness of the SiGe Base region were around 0.21 and 25 nm, respectively.

Cryogenic measurements ranging from 300 to 4.8 K were carried out using a Janis Cryogenic Probe Station ST-500 with liquid helium. The specified operating temperature was precisely controlled by a Model 24C Cryogenic Temperature Controller. All DC measurements in this work performed on an Agilent B1500A Semiconductor Parameter Analyzer. The prepared SiGe HBT wafers were cut into chip dies. The electrical connections between the test die and package were carried out by typical aluminum wire bonding with a diameter of about 25.4 μm. To minimize residual noise, triaxial cables were used to connect the probe station and the Agilent B1500A.

Fig. 2 shows the cross sectional transmission electron microscope (TEM) images of the fabricated SiGe HBT devices. The SiGe base, poly-Si emitter, and contact regions can be clearly seen. For Sample 1, the emitter ploy-Si width W_{EP} and the emitter window width W_E were 1.5 and 0.85 μm, respectively. For Sample 2, shallow trench isolation was applied, and the W_{EP} and W_E were 0.55 and 0.25 μm, respectively. These results are consistent with the device design specifications described above.

3. Analytical model description

We derive the expressions of turn-on voltage (V_{on}, defined as $V_{on} = V|_{J=J_{on}}$) of BE and BC junctions as a function of measurement temperature. Junction current-voltage (*I-V*) characteristics of the prepared HBT samples were measured from 300 to 4.8 K, where the collector was open for the BE junction *I-V* measurement (the emitter was open for the BC junction measurement). The junction current density J is then normalized by A_E (A_C).

3.1. V_{on} - T analytical model for complete ionization

The BE and BC junctions are hetero-structures composed of Ge-induced region and Si region. The traditional Shockley equation is taken as starting in the $V_{on} \sim T$ analytical model. The Ge-induced band offsets and bandgap-narrowing caused by the heavy doping are also taken into consideration.

The most effective dependence of energy bandgap (E_g) on temperature of Si has been shown in Ref. [32]. Because the bandgap of Ge is smaller than that of Si, the Ge-induced band offsets can be written as $\Delta E_g \approx 0.74x_{mol}$, where x_{mol} is the Ge composition. Hence, for the SiGe alloys, $E_{g,SiGe}$ is given by

$$E_{g,SiGe}(T) = E_{g_0,Si} - \frac{\alpha T^2}{T+\varphi} - 0.74x_{mol}, \quad (1)$$

where $E_{g_0,Si}$ is the bandgap of Si at 0 K, α and φ are material parameters with $\alpha = 4.45 \times 10^{-4}$eV/K, $\varphi = 686$ K.

The most widely used bandgap narrowing (BGN) model is the Slotboom bandgap narrowing model [32–35], which is experimentally determined from the I_C-V_{BE} of NPN bipolar transistors. For heavily doped semiconductor, the Boltzmann statistics are no longer accurate and Fermi-Dirac statistics are applied. The idea of Slotboom BGN model is to decrease artificially the apparent electrical bandgap narrowing $\Delta E_{g,app}$ by $\Delta E_{g,FD}$ (correction to reduce the error introduced by Boltzmann statistics), so that one can continue to apply Boltzmann statistics to describe the heavily doped P-N junction in equilibrium. The apparent bandgap narrowing $\Delta E_{g,app}$ can be given as [33]

$$\Delta E_{g,app} = E_{ref}\left[\ln\left(\frac{N_{tot}}{N_{ref}}\right) + \sqrt{\left(\ln\left(\frac{N_{tot}}{N_{ref}}\right)\right)^2 + 0.5}\right]. \quad (2)$$

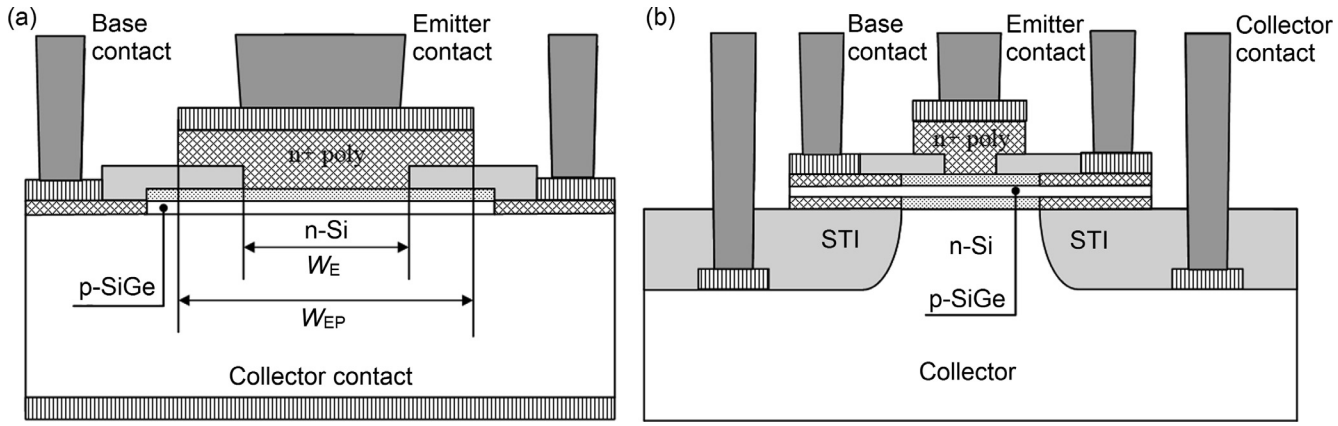

Fig. 1. Schematic cross sections of investigated devices. (a) Sample 1, discrete SiGe HBT. (b) Sample 2, integrated SiGe HBT.

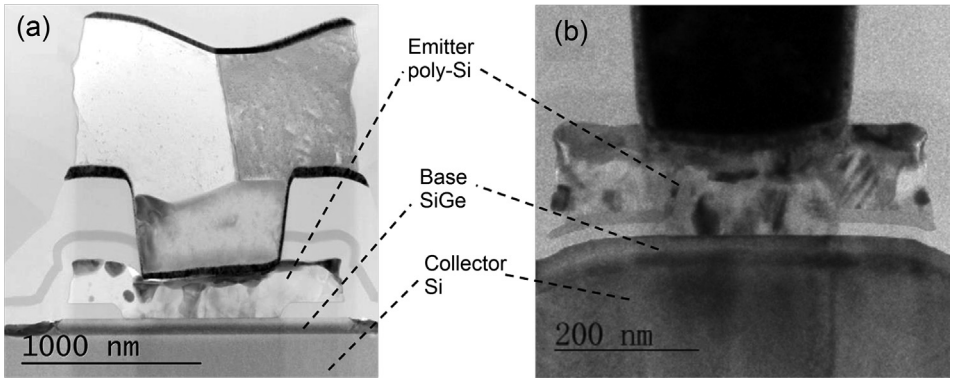

Fig. 2. Cross sectional TEM images of investigated devices. (a) Sample 1. (b) Sample 2.

Hence, the true bandgap narrowing $\Delta E_{g,true}$ can be written as

$$\Delta E_{g,true} = \Delta E_{g,app} - \Delta E_{g,FD}, \tag{3}$$

where $\Delta E_{g,FD}$ is given in Ref. [32], E_{ref} is a constant with 9 meV, N_{tot} is the impurity concentration and N_{ref} is a constant equal to 10^{17} cm^{-3}.

To obtain the dependence of V_{on} on the temperature for the SiGe/Si heterojunctions, we start with the Shockley equation:

$$J = J_s\left[\exp\left(\frac{qV}{NkT}\right) - 1\right], \tag{4}$$

where N is the ideality factor, q is the electron charge, k is the Boltzmann constant, and J_s is the saturation current density [36].

$$J_s = A^* T^2 \exp\left(\frac{-q\Phi_b}{kT}\right), \tag{5}$$

where A^* is the Richardson constant. Φ_b is the barrier height. The effect of temperature on Φ_b is modeled as follow [37]:

$$\Phi_b(T) = \frac{T}{T_{nom}}\Phi_{b,nom} - 3\frac{kT}{q}\ln\left(\frac{T}{T_{nom}}\right) - \left[\frac{T}{T_{nom}}E_{g,SiGe}(T_{nom}) - E_{g,SiGe}(T)\right], \tag{6}$$

where T_{nom} is nominal temperature and has a value of 300 K, Φ_{nom} is the barrier height at T_{nom}.

For $V_{BE} \gg \frac{kT}{q}$, the derivative of base-emitter junction voltage with respect to temperature can be written as

$$\frac{dV}{dT} = \frac{d}{dT}\left[\frac{NkT}{q}\ln\left(\frac{J}{J_s}\right)\right]. \tag{7}$$

By substituting Eqs. (5)–(7), the derivative yields

$$\frac{dV_{on}(T)}{dT} - \frac{V_{on}(T)}{T} = -\frac{2k}{q} + \frac{1}{q}\Phi_b{}' - \frac{\Phi_b}{qT}. \tag{8}$$

The temperature dependence of $E_{g,SiGe}$ and bandgap narrowing are taken into account. Combining Eq. (3), the solution of Eq. (8) is given by

$$V_{on}(T) = \left(\frac{E_{g_0,Si} - 0.74x_{mol} - \Delta E_{g,app}}{q}\right) + BT + \frac{\alpha\varphi T}{q(T+\varphi)} - \frac{2kT}{q}\ln(T), \tag{9}$$

where B is a parameter used during measurement data fitting. The first part relates to the doping concentration and the Ge concentration in base region. In addition, the turn-on current also has an important effect on V_{on}. In order to rectify the model and to fit the experimental result better, the V_{on}-T model is given by

$$V_{on}(T) = A(J_{on}) + B(J_{on})T + \frac{\alpha\varphi T}{q(T+\varphi)} - \frac{2kT}{q}\ln(T), \tag{10}$$

where $A(J_{on})$ is allowed to be an extra fitting parameter, rather than determining from $\frac{E_{g_0,Si} - 0.74x_{mol} - \Delta E_{g,app}}{q}$. The $B(J_{on})$ is a fitting parameter which is related to J_{on}.

3.2. Incomplete ionization

Complete ionization of dopants in Si and SiGe is typically assumed at room temperature. However, when the Fermi level E_F is situated close to the dopant level, the dopant states are noticeably occupied, leading to incomplete ionization even at room temperature [38–40]. The free carrier density is significantly smaller than the dopant density. This semiconductor physics phenomenon is called as the "carrier freeze-out" and shows strong dependence on doping concentration and temperature.

To accurately model the incomplete ionization for heavily doped devices, Mott-transition should be considered with freeze-out model. The ionization rate (IR) is given by the Altemmatt's incomplete ionization model, expressed as [37]

$$IR = \frac{N_D^+}{N_D} = \frac{1}{1 + g_D n/n_1}, \tag{11}$$

$$IR = \frac{N_A^+}{N_A} = \frac{1}{1 + g_A p/p_1}, \tag{12}$$

and

$$n_1 = N_c e^{-E_{dop}/kT}, p_1 = N_v e^{-E_{dop}/kT}, \tag{13}$$

where N_D is the total donor concentration, N_A is the total acceptor concentration, N_D^+ is the ionized donor concentration, N_A^+ is the ionized acceptor concentration, n is the electron density, p is the hole density, E_{dop} is the dopant energy, g_D is the donor degeneracy factor, and g_A is the acceptor degeneracy factor [39].

Fig. S1 (online) shows the calculated temperature dependence of IR with different doping concentrations for arsenic (As), phosphorus (P) and boron (B), respectively. At $N_{dop} = 1 \times 10^{18}$ cm^{-3}, ionization rate is incomplete and decreases with the temperature cooled. As the doping concentration increases, the carrier freeze-out effect decreases gradually. When the doping concentration achieves 1×10^{20} cm^{-3}, the ionization remains complete even when the temperature goes down.

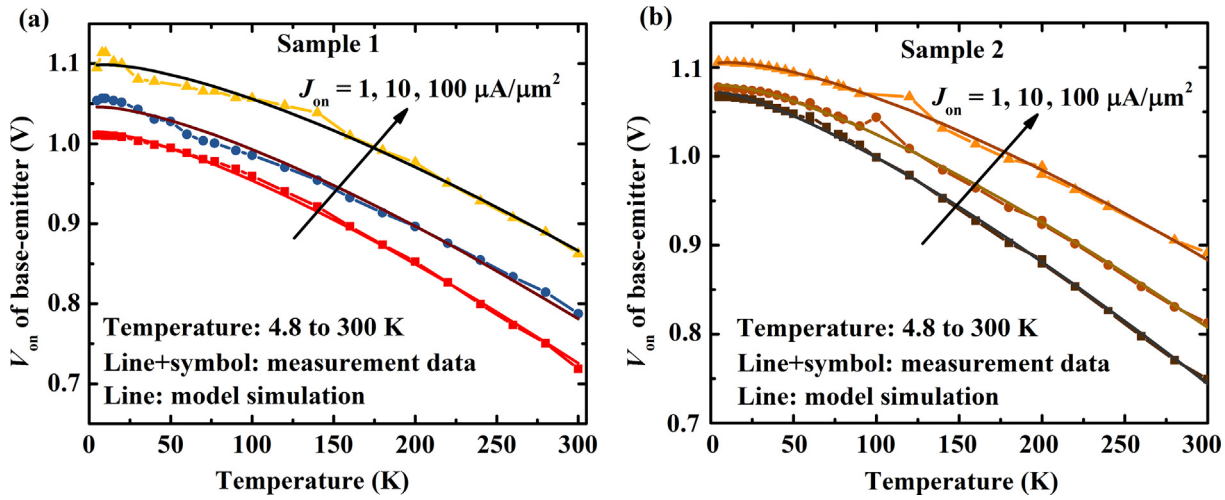

Fig. 3. (Color online) The extracted temperature dependence of V_{on} of BE junction. Symbols represent numerical simulation and lines represent analytical model. (a) Sample 1. (b) Sample 2.

3.3. V_{on} extraction and analysis

Fig. 3 presents the extracted V_{on} of BE junctions at different J_{on}, which increases almost linearly as the temperature decreases from room temperature to 160 K. Below 160 K, however, the slope of V_{on} increase gradually reduces to about zero, possibly due to the band-gap energy increasing as the temperature goes further down. Due to the heavy doping in emitter and p-SiGe base of HBTs, the impurity is almost completely ionized even if the temperature cools down to 4.8 K (Fig. S1 online). Hence, the V_{on}-T analytical model proposed in Section 3.1 can be used to illustrate the turn-on characteristics of the BE junction for these two measured HBT devices. The results of the model simulation are shown in Fig. 3. Table S1 (online) shows the fitting parameters of the V_{on}-T analytical model. The average slope $\Delta V_{on}/\Delta T$ of V_{on}-T in full temperature range (4.8 to 300 K) is defined as $(V_{on,T_{max}} - V_{on,T_{min}})/(T_{max} - T_{min})$, where the $\Delta V_{on}/\Delta T$ is around -1 ± 0.1 mV/K.

Fig. S2 (online) shows the extracted V_{on} of the BC junction. It is apparent that a considerable V_{on} increase occurred from 180 to 4.8 K for Sample 1 and from 50 to 4.8 K for Sample 2. The complete ionization V_{on}-T analytical model described above is no longer suited for this situation. This is possibly caused by the carrier freeze-out due to the lower doping concentration of the collector region comparing with the doping concentration at Mott-transition.

4. Devices comparison and discussion

4.1. Gummel characteristics

To characterize the features of these SiGe HBTs across the cryogenic temperature range, the Gummel characteristics ($V_{CB} = 0$ V) were measured from 300 to 4.8 K, as shown in Fig. 4. Due to the Ge-induced profile and the heavy doping in the base region, these measured SiGe HBTs exhibited excellent transistor-like behavior with sizeable current gain at cryogenic temperature. When the temperature decreased, both I_C and I_B curves began to shift to higher operating voltages. Below 20 K, however, the curves essentially overlapped each other even if the temperature continuously cooled down.

It is obvious that a non-ideal base current component in the forward mode existed below 20 K, as shown in Fig. 4. This non-ideal base current is related to the heavy doping nature of the base-emitter, which is called trap-assisted tunneling (TAT) current [41,42]. Due to the decreasing defect density in the state-of-art device fabrication, the TAT current is typically negligible at room temperature. However, as the temperature decreases, the regular diffusion current reduces rapidly, while the TAT current does not decrease as much.

To illustrate the difference between these two measured SiGe HBTs, this work used the I_C-V_{BE} model [43], which is expressed as

$$I_C = \frac{I_s}{q_B}\left[\exp\left(\frac{V_{BE}}{N_F V_T}\right) - 1\right], \tag{14}$$

where I_s is the saturation current, q_B is the normalized majority base charge for HBTs, N_F is the ideality factor, and $V_T = KT/q$. The models of I_s and N_F as a function of temperature have been given in ref. [43].

Fig. 5 shows the extracted results and model simulation of I_s and N_F from 300 to 40 K. The N_F was approaching 2, indicating that the recombination in space charge region contributes to the total collector current besides drift-diffusion current. As the inset shown, however, N_F was much greater than 2 when the temperature went down to 4.8 K. This suggests that the current is not only composed of drift-diffusion and recombination current in space charge region, but also composed of tunneling current [44–48]. The extracted I_s, from 300 to 4.8 K, is also shown in the inset. The I_s of Sample 1 decreases from 2.7×10^{-17} to 1.08×10^{-114} A with the temperature cooled. The I_s of Sample 2 is similar to that of Sample 1 above 40 K. Below 40 K, however, the I_s of Sample 2 tended to flatten with a value of approximate 1×10^{-80} A. The tendency of N_F extracted from these measured devices followed the same trend.

4.2. Current gain

As shown in Fig. 6a, b, current gain ($\beta = I_C/I_B$) extracted from the measured Gummel characteristics varies with collector current density. The range of amplifying region becomes narrow as the temperature goes down. In addition, the amplifying region of Sample 2, quantized by collector current density, was obviously wider than that of Sample 1, which resulted from the scaling down of W_{EP} and W_E. The current gain dropped dramatically at high injection region because of the reduction in the voltage caused by parasitic resistances [49].

Peak current gain (β_{Peak}) is the maximum value of β at different temperatures, which is extracted from the $\beta - J_C$ curves. The β_{Peak}

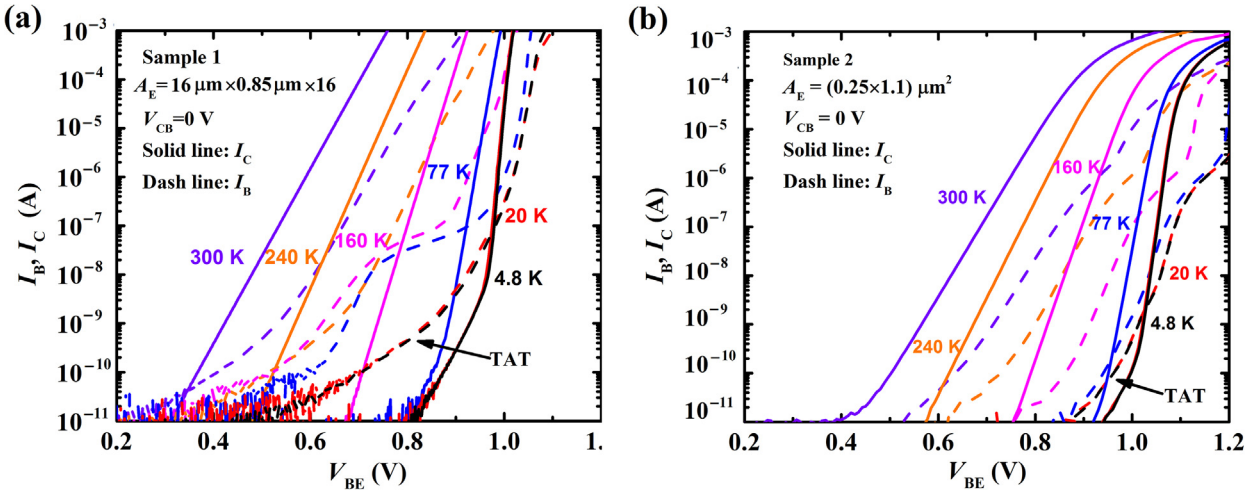

Fig. 4. (Color online) Measured Gummel characteristics of these two SiGe HBTs at 300, 240, 160, 77, 20 and 4.8 K. The Gummel curves at 20 and 4.8 K overlap and are virtually identical. (a) Sample 1; (b) Sample 2.

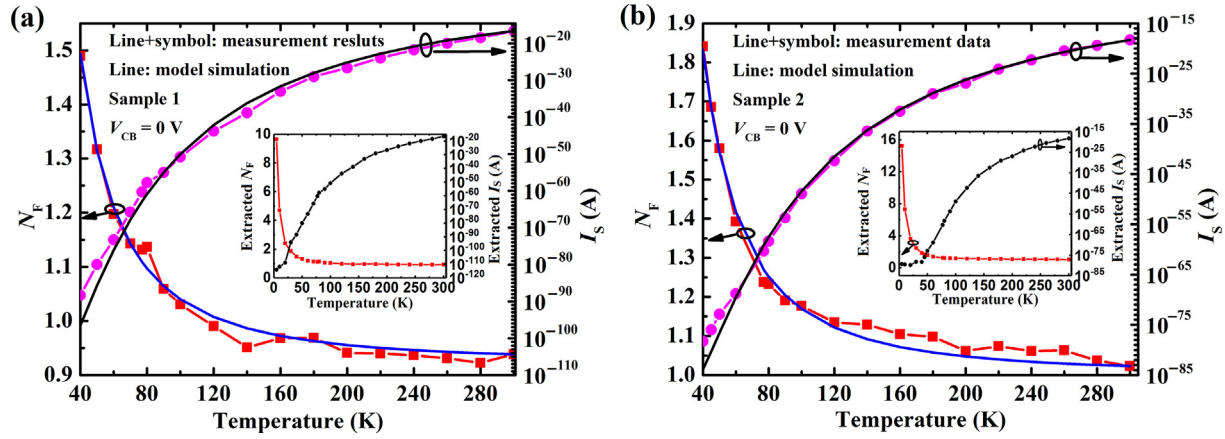

Fig. 5. (Color online) Extracted results and model simulation of ideal factor and saturation current from 300 to 40 K. The inset shows the extracted results from 300 to 4.8 K. (a) Sample 1. (b) Sample 2.

and the corresponding collector current density (J_C for β_{Peak}) and the base current density (J_B for β_{Peak}) are shown in Fig. 6c, d. The β_{Peak} increased exponentially with the temperature cooled from 300 to 80 K for Sample 1 (140 K for Sample 2). Below 80 K for Sample 1 (140 K for Sample 2), however, the exponential increase in the current gain was limited by the parasitic base leakage due to tunneling. The current gain is affected essentially by the different functions of J_C and J_B versus temperature. As shown in Fig. 6c, the maximum β_{Peak} of Sample 1 is located at point A (80 K, 3,388). The J_C for β_{Peak} increases with the temperature down to 90 K (point B) and then decreases. The tendency of J_B for β_{Peak} is similar to J_C, but the maximum value is located at 160 K (point C). Fig. 6d presents the characteristic of Sample 2, whose maximum β_{Peak} is located at point D (140 K, 546). The J_C and J_B for β_{Peak} increase with the temperature decreasing, and the β_{Peak} exactly reflects the discrepancy between J_C and J_B. At 300 K, β_{Peak} are 239 and 314 for Sample 1 and Sample 2, respectively. The difference between two samples is not obvious in this case. However, the current gain of Sample 1 is several times larger than that of Sample 2 with the temperature decreasing, which indicates that the contribution of the temperature effects on these two samples are inconsistent.

Due to the introduction of Ge into the base region, there are two detectable DC consequences by viewing the energy band diagram (Fig. S3a–d online) [50]. Firstly, the potential barrier of electron injection from the emitter into the base decreased. Secondly, a graded built-in potential in the base region formed because of the compositional gradient of the Ge profile, which decreases the transit time when electrons transport across the base region. These two effects resulted in a higher current and hence a higher current gain. The measured Ge and Si composition of Sample 1 is shown in Fig. S3e (online). And the inset of Fig. S3e (online) shows the high-angle annular dark field scanning transmission electron microscopy (HAADF STEM) image of Sample 1, indicating that the line-scan follows the arrow. Sample 2 has a similar Ge profile as Sample 1, but with higher Ge content and much thinner base region. In addition, the current gain of SiGe HBTs also benefits from the bandgap narrowing caused by heavily doped base region.

The carrier mobility affects many factors such as the carrier velocity, drift time across the base region, the emitter injection efficiency, which related to current gain. The most widely used mobility model is the Philips unified mobility model [51–53], which unifies the description of majority and minority carrier bulk motilities. Taking the lattice scattering, impurities scattering, electron-hole scattering and impurity screening into account, the mobility can be given by

$$\frac{1}{\mu_{e,h}} = \frac{1}{\mu_L} + \frac{1}{u_{DAeh}}, \tag{15}$$

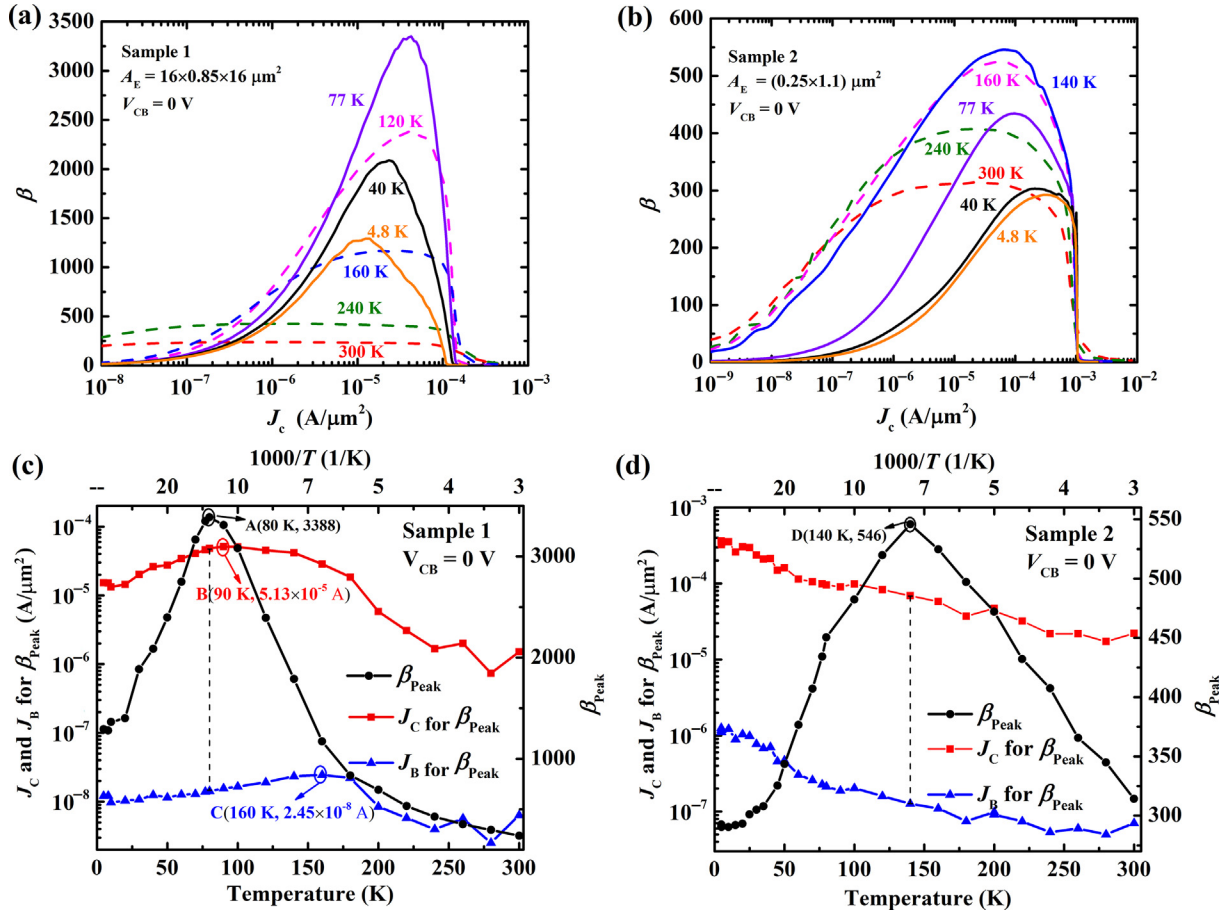

Fig. 6. (Color online) The characteristics of current gain extracted from Gummel curves. β of Sample 1 (a) and Sample 2 (b) as a function of J_C at different temperatures. (c) β_{Peak} and the corresponding J_C and J_B of Sample 1 (c) and Sample 2 (d) for specified β_{Peak} versus temperature.

where μ_L represents the lattice scattering contribution, and μ_{DAeh} accounts for all other bulk scattering mechanisms due to free carriers, ionized donors and acceptors [51,53].

The carrier mobility in Si bulk simulated by Eq. (15) is shown in Fig. S4 (online). Further works about carrier mobility in SiGe bulks have been reported [54–60]. The carrier mobility is affected by impurities, doping concentration, and temperature. The mobility decreases as the doping concentration increases and has a negative correlation with the temperature. The difference between J_C and J_B results from the carriers' different level of sensitivity to temperature. Meanwhile, the mobility and carrier concentration, which both affect the operating current, are dependent on incomplete ionization at low temperature.

Hence, the emitter injection efficiency γ_E is used to illustrate the combined action on current gain, which is given as [61]

$$\gamma_E = \frac{1}{1 + \left(\frac{D_E}{D_B}\right)\left(\frac{L_B}{L_E}\right)\left(\frac{N_B}{N_E}\right)\tanh\left(\frac{W_B}{L_B}\right)}, \tag{16}$$

where L_B and L_E are the equilibrium minority carrier diffusion lengths in the base and emitter region respectively, W_B is the base width, D_E and D_B are the diffusion efficiency in the emitter and base, related to the carrier mobility. N_B and N_E are the base doping and emitter doping. When the temperature cools down, the N_B and N_E are replaced with ion concentrations which are determined by ionization rate. Due to the difference of process fabrication parameters, the temperature effects on mobility and ionization rate of these two samples are inconsistent with each other, which are the critical reasons why the current gain of Sample 1 is several times larger than that of Sample 2.

The operating characteristics of SiGe HBTs depend on physical parameters, such as Ge composition and doping concentration analyzed above. Fig. S5 (online) illustrates the current gain of the investigated SiGe HBTs with different technologies in this work comparing to the literatures [21–23]. The β_{Peak} of measured devices in Ref. [21,22] increased as the temperature cooled down. A fourth

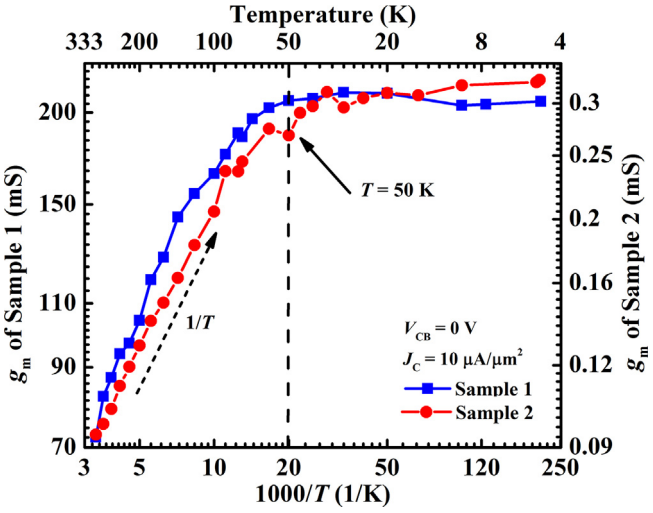

Fig. 7. (Color online) Transconductance (g_m) in logarithmic scale as a function of reciprocal temperatures. g_m is extracted at J_C = 10 μA/μm² from 300 to 4.8 K.

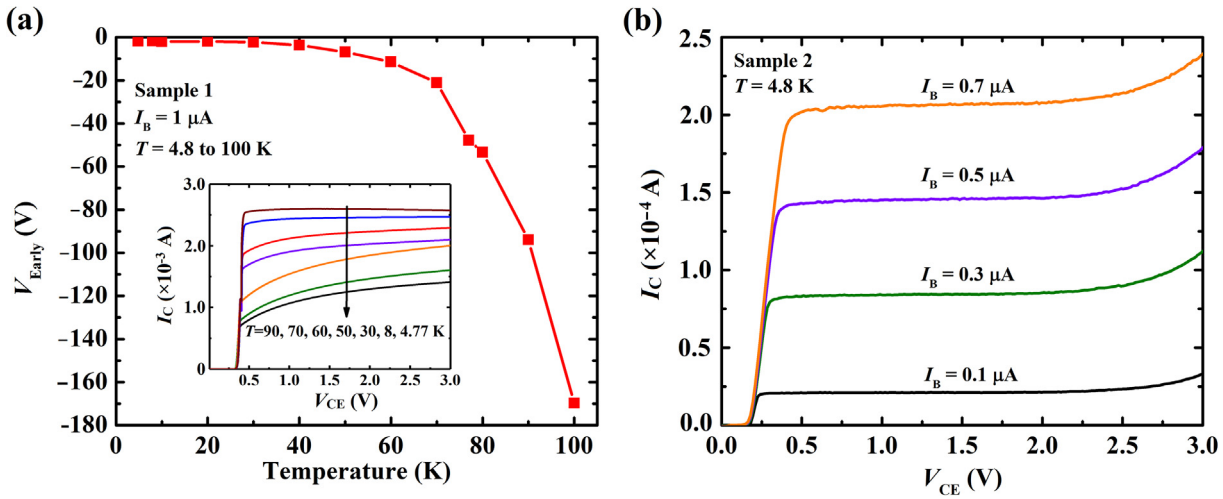

Fig. 8. (Color online) The early effect on these two samples. (a) The extracted early voltage versus temperature of Sample 1. Inset shows the measured Forced-I_B output characteristics of Sample 1 from 100 to 4.8 K. (b) Forced-I_B output characteristics of Sample 2 at 4.8 K with different base currents.

generation, highly scaled, 90-nm SiGe HBT can operate at cryogenic temperature as low as 70 mK. The tendency of β at $I_C = 1$ μA is reported [23] and is similar to that of Sample 2.

Finally, V_{BE} for β_{Peak} ($V_{BE,\beta_{Peak}}$) is shown in Fig. S6 (online), which is significant for circuit design. We define the knee point as knee voltage ($V_{BE,Knee}$), where $\frac{d\ln(J_C)}{dV_{BE}} \propto \frac{q}{2N_F V_T}$. When $V_{BE} > V_{BE,Knee}$, the linearity is not good enough for circuit design, especially for amplifier design. Fig. S6 (online) shows the temperature dependence of $V_{BE,Knee}$. When the temperature decreased to 100 K, the β_{Peak} points of both samples were above the knee point. This suggests that the operating point of the circuit design should be selected below the knee point to obtain higher linearity.

4.3. Transconductance

The transconductance (g_m) is plotted versus the reciprocal temperature in Fig. 7, where collector current density J_c is 10 $\mu A/\mu m^2$. When these devices work in ideal forward-active regions, Eq. (14) can be used to describe the $I_C - V_{BE}$ curves. Hence, g_m is given by

$$g_m = \frac{dI_C}{dV_{BE}} = \frac{I_S}{q_B}\frac{1}{N_F V_T}\exp\left(\frac{V_{BE}}{N_F V_T}\right), \quad (17)$$

where N_F is a function of temperature. Above 50 K, N_F is less than 2. The $\ln(g_m)$ is linearly dependent on $1/T$, which agrees with the drift-diffusion theory. Below 50 K, however, $\ln(g_m)$ tends to flatten, indicating that the collector current no longer has a strong correlation with the temperature. This phenomenon suggests the presence of non-equilibrium transport mechanisms that can be attributed to the carriers' quasi-ballistic transport through the neutral base region and higher effective electron temperature compared with the lattice temperature [23,62].

4.4. Output characteristics

To study the performance between discrete and integrated SiGe HBTs measured in this work, the output characteristic is another critical considered factor. Force-I_B output characteristics were measured from 300 to 4.8 K. Fig. 8a shows the early voltage (V_{Early}) of Sample 1 extracted from Force-I_B output curves at fixed $I_B = 1$ μA. Below 77 K, V_{Early} gradually approached −2 V with the temperature down to 4.8 K. Above 77 K, absolute value of V_{Early} exponentially increases. The inset figure presents the output characteristics at different temperatures. However, the early voltage of Sample 2 did not vary with temperature obviously. Fig. 8b illustrates the output characteristics of Sample 2 with fixed $I_B = 0.1$ to 0.7 μA at 4.8 K.

5. Conclusion

We investigated the performance discrepancy between the discrete SiGe HBTs and the integrated SiGe HBTs over a wide temperature range from 300 to 4.8 K. The V_{on} of BE and BC junction increased non-linearly with the temperature cooled. A V_{on}-T analytical model was developed to illustrate this tendency of BE junction. However, due to incomplete ionization in the BC junction, a knee point appeared in the extracting V_{on} curves. The Gummel plots at $V_{CB} = 0$ V were shifted to higher operating voltage when the temperature decreased. In addition, the TAT current was dominant at low V_{BE} below 20 K. An $I_C - V_{BE}$ model was used to characterize the Gummel characteristics, where the current gain was obtained from the Gummel curves. Energy band diagram and Philips unified mobility model were used to analyze the temperature dependence of current gain. The knee voltage and V_{BE} for β_{Peak}, which are critical factors in circuit design, showed that the linearity gradually decreased with the temperature cooled. The $\ln(g_m)$ was linearly dependent on $1/T$ above 50 K, but tended to flatten from 50 K down to 4.8 K. Finally, the measured output characteristics indicated that the early effect was more obvious in Sample 1 than Sample 2. These results suggest an effective way to research the performance of SiGe HBTs at cryogenic temperature and to further investigate cryogenic circuit design.

Conflict of interest

The authors declare that they have no conflict of interest.

Acknowledgments

This work was supported by the National Key Research and Development Program of China (2016YFA0200300, 2016YFA0200400), the National Science and Technology Major Project of China (2016ZX02301001), the National Natural Science Foundation of China (61574083, 61434001), the National Basic Research Program of China (2015CB352101), Special Fund for Agroscientific Research in the Public Interest of China (201303107), and Research Fund from Beijing Innovation Center

for Future Chip. The authors are also thankful for the support of the Independent Research Program of Tsinghua University (2014 Z01006), Beijing Natural Science Foundation (4184091), and Shenzhen Science and Technology Program (JCYJ2015083119 2224146).

Author contributions

Guofang Yu, Renrong Liang, Jun Xu, and Tian-Ling Ren conceived and designed the experiments. Guofang Yu and Renrong Liang performed the experiments and analyzed the data. Guofang Yu, Renrong Liang, Xiawa Wang, Jun Xu, and Tian-Ling Ren performed the analysis with constructive discussions. Guofang Yu, Renrong Liang, Jun Xu, and Tian-Ling Ren contributed to the conception of the study.

Appendix A. Supplementary data

Supplementary data to this article can be found online at https://doi.org/10.1016/j.scib.2019.03.005.

References:

[1] Cornett KJ, Fu G, Escorcia I, et al. SiGe BiCMOS fully differential amplifier for extreme temperature range applications. IEEE Aero Conf 2009:1–10.
[2] Groves III WM, Morgan MA. A cryogenic SiGe low-noise amplifier optimized for phased-array feeds. Publ Astron Soc Pac 2017;129:85001.
[3] Bryerton EW, Morgan M, Pospieszalski MW. Ultra low noise cryogenic amplifiers for radio astronomy. IEEE Radio Wireless Symp 2013:358–60.
[4] Montazeri S, Wong W, Coskun AH, et al. Ultra-low-power cryogenic SiGe low-noise amplifiers: theory and demonstration. IEEE T Microw Theory 2016;64:178–87.
[5] Thrivikraman TK, Yuan J, Bardin JC, et al. SiGe HBT X-band LNAs for ultra-low-noise cryogenic receivers. IEEE Microw Wirel Co 2008;18:476–8.
[6] Kiviranta M. Use of SiGe bipolar transistors for cryogenic readout of SQUIDs. Supercond Sci Technol 2006;19:1297–302.
[7] Luo L, Niu G, Moen KA, et al. Compact modeling of the temperature dependence of parasitic resistances in SiGe HBTs down to 30 K. IEEE T Electron Dev 2009;56:2169–77.
[8] Joseph AJ, Cressler JD, RicheY DM. Operation of SiGe heterojunction Bipolar-transistors in the liquid-helium temperature regime. IEEE Electr Device L 1995;16:268–70.
[9] Najafizadeh L, Adams JS, Phillips SD, et al. Sub-1-K operation of SiGe transistors and circuits. IEEE Electron Device L 2009;30:508–10.
[10] Varonen M, Reeves R, Kangaslahti P, et al. An MMIC low-noise amplifier design technique. IEEE T Microw Theory 2016;64:826–35.
[11] Varonen M, Reeves R, Kangaslahti P, et al. A 75–116-GHz LNA with 23-K noise temperature at 108 GHz. IEEE MTT-S Int Microwave Symp Dig 2013:1–3.
[12] Cha E, Moschetti G, Wadefalk N, et al. Two-finger InP HEMT design for stable cryogenic operation of ultra-low-noise Ka- and Q-band LNAs. IEEE T Microw Theory 2017;65:5171–80.
[13] Dogmus E, Kabouche R, Lepilliet S, et al. InAlGaN/GaN HEMTs at Cryogenic Temperatures. Electronics 2016;5:31.
[14] de la Broïse X, Bounab A. Cryogenic ultra-low noise HEMT amplifiers board. Nucl Instrum Meth 2015;787:51–4.
[15] Dong Q, Liang YX, Ferry D, et al. Ultra-low noise high electron mobility transistors for high-impedance and low-frequency deep cryogenic readout electronics. Appl Phys Lett 2014;105:13504.
[16] de la Broïse X, Lugiez F, Bounab A, et al. Cryogenic low noise and low dissipation multiplexing electronics, using HEMT+SiGe ASICs, for the readout of high impedance sensors: new version. Nucl Instrum Meth 2015;787:64–7.
[17] Arakawa T, Nishihara Y, Maeda M, et al. Cryogenic amplifier for shot noise measurement at 20 mK. Appl Phys Lett 2013;103:172104.
[18] Schleeh J, Wadefalk N, Nilsson P, et al. Cryogenic broadband ultra-low-noise MMIC LNAs for radio astronomy applications. IEEE T Microw Theory 2013;61:871–7.
[19] Neilinger P, Trgala M, Grajcar M. Cryogenic low noise 2.2–3 GHz amplifier. Cryogenics 2012;52:362–5.
[20] Cressler JD, Niu G. Silicon-germanium heterojunction bipolar transistors. Boston, MA: Artech House; 2003.
[21] Yuan J, Cressler JD, Krithivasan R, et al. On the performance limits of cryogenically operated sige hbts and its relation to scaling for terahertz speeds. IEEE T Electron Dev 2009;56:1007–19.
[22] Cressler JD. On the potential of sige hbts for extreme environment electronics. P IEEE 2005;93:1559–82.
[23] Ying H, Wier BR, Dark J, et al. Operation of SiGe HBTs down to 70 mK. IEEE T Electron Dev 2017;38:12–5.
[24] Janzen A, Weinreb S. Manufacturable cryogenic SiGe LNA for radio astronomy and space communications. USNC-URSI NRSM 2016:1–2.
[25] Smith S, Weinreb S. A cryogenic, wide band receiver for the 500 m aperture spherical telescope (FAST). IEEE URSI AP-RASC 2016:1595–8.
[26] Weinreb S, Bardin JC, Mani H. Design of cryogenic SiGe low-noise amplifiers. IEEE T Microw Theory 2007;55:2306–12.
[27] Russell D, Weinreb S. Low-power very low-noise cryogenic SiGe IF amplifiers for terahertz mixer receivers. IEEE T Microw Theory 2012;60:1641–8.
[28] Bardin JC, Weinreb S. A 0.1–5 GHz cryogenic SiGe MMIC LNA. IEEE Microw Wirel Co 2009;19:407–9.
[29] Curry MJ, England TD, Bishop NC, et al. Cryogenic preamplification of a single-electron-transistor using a silicon-germanium heterojunction-bipolar-transistor. Appl Phys Lett 2015;106:541–612.
[30] Banerjee B, Venkataraman S, Lu Y, et al. Cryogenic operation of third-generation, 200-GHz Peak-fT, Silicon-Germanium Heterojunction Bipolar Transistors. IEEE T Electron Dev 2005;52:585–93.
[31] Banerjee B, Venkataraman S, Lu Y, et al. Cryogenic performance of a 200 GHz SiGe HBT technology. IEEE BCTM 2003:171–3.
[32] Physics Luo L. Compact Modeling and TCAD of Silicon Germanium HBT for Wide Temperature Range Operation. In. Ann Arbor: Auburn University 2011:243.
[33] Slotboom J, Graaff H. Measurements of bandgap narrowing in Si bipolar transistors. Solid State Electron 1976;19:857–62.
[34] Yao F, Xue CL, Cheng BW, et al. Bandgap narrowing in heavily B doped $Si_{1-x}Gex$ strained layers. Acta Phys Sin 2007;56:6654–9.
[35] Van Cong H. Bandgap changes in excited intrinsic (heavily doped) Si and Ge semiconductors. Phys B 2010;405:1139–49.
[36] Deb P, Kim H, Qin Y, et al. GaN nanorod Schottky and p-n junction diodes. Nano Lett 2006;6:2893–8.
[37] Antognetti P, Massobrio G. Semiconductor device modeling with spice. New York: McGraw-Hill Inc; 1988.
[38] Altermatt PP, Schenk A, Heiser G. A simulation model for the density of states and for incomplete ionization in crystalline silicon. I. Establishing the model in Si: P. J Appl Phys 2006;100:113714.
[39] Altermatt PP, Schenk A, SchmithÜsen B, et al. A simulation model for the density of states and for incomplete ionization in crystalline silicon. II. Investigation of Si: As and Si: B and usage in device simulation. J Appl Phys 2006;100:113715.
[40] Forster M, Rougieux FE, Cuevas A, et al. Incomplete ionization and carrier mobility in compensated p-type and n-type silicon. IEEE J Photovolt 2013;3:108–13.
[41] Xu Z, Niu G, Luo L, et al. A physics-based trap-assisted tunneling current model for cryogenic temperature compact modeling of SiGe HBTs. ECS Trans 2010;33:301–10.
[42] Luo L, Xu Z, Niu G, et al. Wide temperature range compact modeling of SiGe HBTs for space applications. Mccarthy 2011:110–3.
[43] Xu Z, Wei X, Niu G, et al. Modeling of Temperature Dependent I-C-V-BE Characteristics of SiGe HBTs from 43–400 K. IEEE BCTM 2008:81–4.
[44] Modi BP, Dhimmar JM. The temperature dependent ideality factor effect on *I-V* characteristics of Schottky diode. ET2ECN 2012.
[45] Wang C, Yang G, Liu H, et al. Experimental analysis and theoretical model for anomalously high ideality factors in ZnO/diamond p-n junction diode. Appl Phys Lett 2004;84:2427–9.
[46] Verschraegen J, Burgelman M, Penndorf J. Temperature dependence of the diode ideality factor in $CuInS_2$-on-Cu-tape solar cells. Thin Solid Films 2005;480-481:307–11.
[47] Jyothi I, Seo MW, Janardhanam V, et al. Temperature-dependent current–voltage characteristics of Er-silicide Schottky contacts to strained Si-on-insulator. J Alloy Compd 2013;556:252–8.
[48] Simeonov SS, Kafedjiiska E, Szekeres A, et al. Trap-assisted tunneling at temperatures near 77 K in laser annealed Si n^+-p junctions. J Appl Phys 2001;90:860.
[49] Ashburn P. SiGe heterojunction bipolar transistors. Hoboken, NJ: John Wiley & Sons Ltd; 2003.
[50] Sah CT. Fundamentals of Solid-State Electronics. Singapore: World Scientific; 1991.
[51] Klaassen D. A unified mobility model for device simulation--I. Model equations and concentration dependence. Solid State Electron 1992;35:953–9.
[52] Forster M, Rougieux FE, Cuevas A. Incomplete ionization and carrier mobility in compensated p-type and n-type. Silicon. IEEE J Photovolt 2013;3:108–13.
[53] Klaassen DBM. A unified mobility model for device simulation—II. Temperature dependence of carrier mobility and lifetime. Solid State Electron 1992;35:961–7.
[54] Murphy-Armando F, Fahy S. First principles calculation of electron-phonon and alloy scattering in strained SiGe. J Appl Phys 2011;110:123706.
[55] Romano L, Napolitani E, Privitera V, et al. Carrier concentration and mobility in B doped $Si_{1-x}Ge_x$. Mater Sci Eng B 2003;102:49–52.
[56] Sasso G, Rinaldi N, Matz G, et al. Analytical models of effective DOS, saturation velocity and high-field mobility for SiGe HBTs numerical simulation. Proc SISPAD 2010:279–82.
[57] Yang H, Wang D, Nakashima H. Influence of SiGe layer thickness and Ge fraction on compressive strain and hole mobility in a SiGe-on-insulator substrate fabricated by the Ge condensation technique. Thin Solid Films 2012;520:3283–7.
[58] Reiche M, Moutanabbir O, Hoentschel J, et al. Strained silicon devices. Solid State Phenom 2009;156–158:61–8.

[59] Sasso G, Rinaldi N, Matz G, et al. Accurate mobility and energy relaxation time models for SiGe HBTs numerical simulation. Proc SISPAD 2009:241–4.
[60] Smirnov S, Kosina H, Selberherr S. Investigation of the electron mobility in strained $Si_{1-x}Ge_x$ at high Ge composition. IEICE T Electron 2003;86:350–6.
[61] Wu X, Maimon S, Averett KL, et al. Emitter injection efficiency and base transport factor in InAs bipolar transistors. J Appl Phys 2003;94:5423.
[62] Danilchenko BA, Tripachko NA, Belyaev AE, et al. High-field quasi-ballistic transport in AlGaN/GaN heterostructures. Appl Phys Lett 2014;104:195.

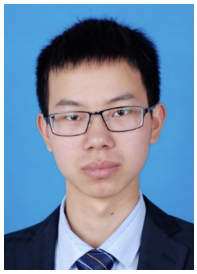

Guofang Yu received the B.S. degree in electronics science and technology from Southeast University in 2012. He is currently a graduate student at Institute of Microelectronics, Tsinghua University. His research concentrates on the low temperature characteristics and models of SiGe material-based devices.

Renrong Liang received the Ph.D. degree in electronics science and technology from Tsinghua University in 2008. As an assistant professor with the Institute of Microelectronics at Tsinghua University, his current research interests are concerned with fabrication and simulation of SiGe and 2D materials-based devices, transport models and optimization of low-power nanoscale MOS devices, such as strained Si MOSFETs, FinFETs, tunneling FETs and negative capacitance FETs, and device physics.